

The nature of the maximum microhardness and thickness of the gradient layer in surface-strengthened Cu-Al alloys

C. X. Ren ^{a, b}, Q. Wang ^{a*}, J. P. Hou ^a, Z. J. Zhang ^a, Z. F. Zhang ^{a, b*}, T. G. Langdon ^c

^a *Shi-changxu Innovation Center for Advanced Materials, Institute of Metal Research, Chinese Academy of Sciences, Shenyang 110016, PR China*

^b *School of Materials Science and Engineering, University of Science and Technology of China, Shenyang 110016, PR China*

^c *Department of Mechanical Engineering, University of Southampton, Southampton SO17 1BJ, UK*

Abstract

The presence of a gradient layer with an increased maximum microhardness and extended thickness is extremely attractive because it can enhance the server performances for surface-strengthened metallic materials. In this work, Cu-Al alloys with different Al contents and microstructures were processed by surface spinning strengthening (3S) and studies were conducted to examine the microstructure and mechanical properties of the as-received Cu-Al alloys together with the gradient microstructure and microhardness distributions of the 3S Cu-Al alloys. The experimental results show that each group of 3S Cu-Al alloys having the same Al content has approximately the same maximum microhardness at the topmost surface of the gradient layers and the maximum microhardness increases with an increase in the Al content. In addition, the thickness of the gradient layer in the 3S Cu-Al alloys increases with a decrease of yield strength and an increase in the work-hardening exponent, respectively. The relationship between the maximum microhardness and chemical composition which determines the Young's modulus and plastic deformation mode, and the relationship between the thickness of the gradient layer and the microstructure which governs the strength and work-hardening capacity, were both investigated. It is shown that the maximum microhardness of the gradient layer depends mainly on the chemical composition and is less related to the microstructure; whereas the thickness of the gradient layer depends primarily on the strength and work-hardening capacity and is closely related to the microstructure and independent of the chemical composition. By combining the compositional design and microstructure optimization of the as-received materials, and improving the surface strengthening intensity, a gradient layer of the surface-strengthened materials with an enhanced maximum microhardness and an extended thickness may be achieved.

Keywords: Cu-Al alloy; Gradient layer; Microhardness; Microstructure; Surface

* Corresponding authors, E-mail: gmwang@imr.ac.cn (Q. Wang), zhfzhang@imr.ac.cn (Z. F. Zhang)

spinning strengthening; Yield strength.

1. Introduction

Surface mechanical strengthening, which can create gradient microstructure and gradient mechanical properties in the surface layers of metallic materials, may effectively enhance the service performance of components and therefore it has attracted much attention over the last decade [1-3]. Investigations of the gradient layer focus primarily on the gradient structures which include the gradient nanogained, nanolaminated and nanotwinned structures [4-6] and the surface strengthening mechanisms include plastic deformation and grain refinement by dislocation subdivision and twinning fragmentation [7, 8]. The microhardness and compressive residual stress distributions in the gradient layers are also involved because they are related to the formation of gradient microstructures and they affect the gradient mechanical properties. The mechanical properties of surface-strengthened materials with gradient layers have been investigated, such as the tensile, wear and fatigue properties [8, 9]. As the gradient layer has an enhanced strength and the remaining matrix maintains the original strength and ductility, surface-strengthened metals with gradient layers provide a clear improvement in yield strength with only a small sacrifice in ductility. An example is the AISI 304 stainless steel with a gradient nanostructure processed by surface mechanical attrition treatment (SMAT) [10]. Due to the introduction of the gradient layer with an improved microhardness, the wear resistance of surface-strengthened metals is greatly improved. Thus, the wear loss of an AISI D2 tool steel was decreased after an ultrasonic impact treatment (UIT) [11]. Moreover, there are enhanced fatigue properties including a suppression of fatigue crack initiation and an increased fatigue life, as in a Ti-6Al-4V alloy processed by ultrasonic SMAT [12]. and a 50CrMnMoVNb spring steel processed by surface spinning strengthening (3S) [13].

For surface-strengthened metals, the key parameter for achieving enhanced tensile properties and service performance is to determine a procedure for constructing a gradient layer which effectively controls the properties. When constructing a gradient

layer, the grain size distribution, the dislocation density, the grain boundary (GBs) and twin boundary (TBs) densities along the depth direction are changeable and vary with the method of surface mechanical strengthening and the type of metal [14-16]. Correspondingly, the properties of the gradient layer, such as the maximum microhardness and the thickness of the gradient layer, exhibit significant differences. For the same material processed by different surface strengthening methods, the gradient properties are generally similar but there are some differences which may be associated with the different surface strengthening intensities. For instance, pure copper processed by platen friction sliding deformation produced a gradient layer with a thickness of $\sim 2000 \mu\text{m}$ and a maximum microhardness of $\sim 2.28 \text{ GPa}$ on a base of $\sim 1.04 \text{ GPa}$ [17], whereas a pure copper processed by high-pressure surface rolling (HPSR) exhibited a gradient layer with a thickness of $\sim 1760 \mu\text{m}$ and a maximum microhardness of $\sim 1.9 \text{ GPa}$ on a base of $\sim 0.8 \text{ GPa}$ [18].

For different materials processed by the same surface strengthening method, the properties of the gradient layers exhibit significant differences which are mainly affected by the material properties. Thus, an SAE 1045 steel after shot peening (SP) treatment gave a gradient layer with a thickness of $\sim 200 \mu\text{m}$, and a maximum microhardness of $\sim 330 \text{ HV}$ on a base of $\sim 230 \text{ HV}$ [19] while a TRIP780 steel after an SP treatment gave a gradient layer with a thickness of $\sim 150 \mu\text{m}$ and a maximum microhardness of $\sim 415 \text{ HV}$ on a base of $\sim 260 \text{ HV}$ [20]. It was also found that both the maximum microhardness and the thickness of the gradient layers of four structural steels gradually increased with the increasing strength of the materials after a 3S treatment with the same parameters [21].

It is generally difficult to obtain a thicker gradient layer since the maximum microhardness increases compared to the matrix microhardness during any surface mechanical strengthening for high-strength metals. By contrast, low-strength metals are easily surface strengthened to give thicker gradient layers but the values of the increases in the maximum microhardness are lower than for high-strength metals. Although some research has been conducted to study the gradient layers of different materials treated by different surface strengthening methods, the precise nature of the gradient layer,

including the maximum microhardness and thickness, are not well defined for surface-strengthened metals. Furthermore, the characteristics and evaluations of the maximum microhardness and the thickness of the gradient layer lack a detailed systematic investigation. In the present research, Cu-Al alloys having different Al contents were employed as model materials and then subjected to a 3S treatment to reveal the properties of the gradient layer including the maximum microhardness and the thickness of the gradient layer. Thus, the overall objective was to explore the rules governing the properties of the gradient layers and the essential factors associated with the gradient structures that are introduced by surface mechanical strengthening.

2. Experimental material and procedures

2.1. Sample preparation

Cu-Al alloys with three different Al contents, including Cu-5Al, Cu-8Al, and Cu-11Al (at. %), were selected and investigated in this research. After smelting, forging and cold-rolling (CR) treatments, billets were produced with a thickness of ~5 mm for each of the three Cu-Al alloys. The billets of the alloys with different Al contents were divided into six parts and then annealed. The first three parts were annealed at 300 °C, 400°C, and 500 °C with a holding time of 30 min in a salt bath furnace and the cold-rolling and annealing treatments were designated A300, A400 and A500, respectively. The second three parts were annealed at 600 °C, 700°C and 800 °C with a holding time of 1 hr in a box resistance furnace, and the cold-rolling and annealing treatments were designated A600, A700 and A800, respectively. The rolled and annealed Cu-Al alloys were surface strengthened using surface spinning strengthening (3S) with the same parameters and intensities for each alloy. The spinning depth was 450 μm, the rotation speed was 600 rpm and the moving speed was 10 mm/min.

2.2. Microstructure observations

The microstructures of the as-received Cu-Al alloys were observed using a scanning electron microscope (SEM) and an electron back-scattered diffraction (EBSD) technique. The EBSD samples were mechanically ground and then electropolished with a solution of $\text{CO}(\text{NH}_2)_2 + \text{H}_2\text{O} + (\text{CH}_3)_2\text{CHOH} + \text{C}_2\text{H}_5\text{OH} + \text{H}_3\text{PO}_4$ in proportions of

2.5 g, 250 mL, 25 mL, 125 mL and 125 mL, respectively. The microstructures of the 3S Cu-Al alloys were observed by SEM with an electron channeling contrast (ECC) technique. The cross-sectional microstructures of the Cu-Al alloys after the A300, A500 and A800 treatments was observed by SEM-ECC where the preparation of the ECC samples was the same as for the EBSD samples. Both the EBSD and ECC observations were carried out using a LEO Supra 35 field SEM with an operating voltage of 20 kV. The microstructures in the topmost surface layers (about 25 μm from the upper surfaces) were observed after the A300, A500 and A800 treatments using a JEOL 2100F transmission electron microscope (TEM) with an operating voltage of 200 kV. The TEM samples were initially mechanically ground to slices with thicknesses of a ~ 50 μm and then twin-jet electropolished with a solution of $\text{H}_3\text{PO}_4 + \text{C}_2\text{H}_5\text{OH} + \text{H}_2\text{O}$ in volume proportions of 1:1:2 at a temperature of 4~8 $^\circ\text{C}$.

2.3. Mechanical tests and microhardness

Tensile tests of the as-received Cu-5Al (A700), Cu-8Al (A700) and Cu-11Al (A700) samples were conducted in this research and the tensile properties for the other samples were cited from previous work [22]. The tensile samples were cut by wire electrical discharge machining (WEDM) with gauge dimensions of $16 \times 4 \times 5 \text{ mm}^3$, and then mechanically polished using abrasive paper. The tensile testing was conducted using an Instron 5982 testing machine with a contacting Instron extensometer at a strain rate of $1 \times 10^{-3} \text{ s}^{-1}$.

The microhardness distributions in the surface layers of all 3S Cu-Al alloys were measured by mechanically grinding and polishing along the cross-sectional directions and then using a LECO AMH43 automatic microhardness tester fitted with a Vickers indenter. The load was 100 g, and the holding time was 13 s. The distance between the two indentations was 100 μm and the angle between the measurement direction and the depth direction was 30° .

3. Experimental results

3.1. Microstructure of the as-received Cu-Al alloys

By severe plastic deformation and then controlled heat treatments, metallic

materials with fully recrystallized grains may be obtained. For example, Fe-22Mn-0.6C twinning-induced plasticity (TWIP) steel with ultrafine grains [23] and a bulk CoCrFeMnNi high-entropy alloy with recrystallized grains of different grain sizes [24]. In the present work, the three groups of Cu-Al alloys having different Al contents and containing six states in each group were processed by similar cold-rolling and annealing treatments and the microstructural characteristics of these rolled and then annealed Cu-Al alloys were observed by SEM-EBSD. As shown in Fig. 1, all the as-received Cu-Al alloy samples had fully recrystallized grains and the microstructural differences between the samples are described later. For each group of alloys, the grain size increases with an increase in annealing temperature. When the annealing temperature is below 500 °C the grain size increases only slowly but the grain size increases rapidly and some annealing twins are formed when the annealing temperature is increased from 500 °C to 800 °C. As a result, three groups of Cu-Al alloys were prepared having different grain sizes and microstructural characteristics.

3.2. Tensile properties of the as-received Cu-Al alloys

The surface strengthening behavior of metallic materials is closely related to the strength and ductility of the metals obtained by tensile testing [21, 25]. Hence, the tensile engineering stress-strain curves of the as-received Cu-Al alloys are presented in this work. Fig. 2a-c shows the engineering stress-strain curves of Cu-5Al alloys, Cu-8Al alloys and Cu-11Al alloys, respectively. For the Cu-5Al alloys in Fig. 2a, the sample with the A300 treatment has the highest yield strength and ultimate tensile strength and the lowest uniform elongation. With an increase in annealing temperature from A300 to A800 treatments, both the yield strength and the ultimate tensile strength decrease and the uniform elongation increases. For the Cu-8Al alloys in Fig. 2b and Cu-11Al alloys in Fig. 2c, the strength and elongation have the same trend as for the Cu-5Al alloys. However, both the strength and elongation are improved simultaneously when comparing the three groups of Cu-Al alloys with different Al contents after the heat treatment. After the A300 treatment, the yield strength, ultimate tensile strength, and uniform elongation increase in the order of the Cu-5Al, Cu-8Al and Cu-11Al alloys.

Nevertheless, there remains a trade-off between the strength and elongation of each group of Cu-Al alloys after the cold-rolling and annealing treatments but it is apparent that increasing the Al content can break through the trade-off relation between strength and elongation in the Cu-Al alloys. It should be noted that, in addition to the Cu-Al alloys in this work, TWIP steel exhibits a similar relation between strength and elongation. For example, an Fe-31Mn-3Al-3Si TWIP steel had a decreased strength and an increased elongation with an increase in grain size although the trade-off relation between strength and elongation was not broken [26]. Furthermore, a simultaneous improvement of strength and elongation for the Fe-22Mn-0.6C TWIP steel was achieved by adding a nitrogen addition [27].

In addition to strength and ductility, the work-hardening exponent is also an important parameter characterizing the tensile behavior of metallic materials, and this reflects the work-hardening ability and even the compatibility of metals during the plastic deformation. In the present research, the effects of Al content and grain size on the work-hardening ability of the Cu-Al alloys was examined and the relations between the yield strength and work-hardening exponent are shown in Fig. 3. For the Cu-5Al alloy, the work-hardening exponent is very low when the yield strength is high and the work-hardening exponent decreases with an increase in the yield strength. Therefore, there is also an obvious trade-off relation between the work-hardening exponent and the yield strength. Moreover, the work-hardening exponents for both the Cu-8Al and Cu-11Al alloys increase although the yield strengths of these two groups of Cu-Al alloys are higher than for the Cu-5Al alloys. As a result, the trade-off relation between the work-hardening exponent and yield strength is broken by increasing the Al content in the Cu-Al alloys. Taken as a whole, the as-received Cu-Al alloys have a large range of strength, ductility and work-hardening exponent for each group of Cu-Al alloys, and increasing the Al content may break general trade-off relations between the yield strength and uniform elongation and between the yield strength and work-hardening exponent.

3.3. Gradient microstructure of the 3S Cu-Al alloys

A gradient microstructure is the typical microstructural feature of a metal experiencing surface strengthening processing. Concerning the 3S process, the compressive and shear stress are applied onto the surface layer to produce a surface strengthening of metallic materials. In the present research, gradient microstructures of the partial 3S Cu-Al alloys were observed including cross-sectional microstructures in the gradient layers and microstructures in the topmost surface layers. Fig. 4 shows SEM-ECC images for the gradient microstructures of representative 3S Cu-5Al alloys having different matrix grain sizes including after A300, A500 and A800 treatments. The 3S Cu-5Al alloy with the A300 treatment has an obvious gradient microstructure with a distinct grain refinement in the surface layer as shown in Fig. 4a. With an increase in matrix grain size from the A500 to A800 treatments, the thickness of the distinct grain refinement zone in the surface layer increases as shown in Fig. 4b and Fig. 4c. The A800 sample continues to have an obvious grain deformation zone as shown in Fig. 4c and, as a result, the thickness of the grain refinement and grain deformation zone of the 3S Cu-Al alloys increases with an increase in the matrix grain size for each group of alloys.

In addition to a comparison of the gradient microstructures of the 3S Cu-Al alloys with different matrix grain sizes, the effect of Al contents on the gradient microstructure was also examined in this work. Fig. 5 shows SEM-ECC images for the gradient microstructures of the 3S Cu-Al alloys with A800 treatment in the order of the increasing Al content. The Cu-5Al alloy has a distinct gradient characteristic from the topmost surface layer to the matrix direction, especially the gradient grain size as shown in Fig. 5a. The as-received Cu-5Al alloy with the A800 treatment consists of equiaxed coarse grains and some annealing twins as shown in Fig. 1a but the microstructure in the surface layer with a thickness of $\sim 700 \mu\text{m}$ for the 3S sample consists of refined grains and deformed grains. Thus, the grain refinement and grain deformation are more severe closer to the topmost surface. For the 3S Cu-8Al alloy with the A800 treatment as shown in Fig. 5b and the Cu-11Al alloy with the A800 treatment as shown in Fig. 5c,

the microstructures in the surface layers have similar characteristics to the Cu-5Al alloy with the A800 treatment. As a result, there are similar gradient characteristics in the surface layers for the three groups of Cu-Al alloys having the same heat treatments after the 3S process.

In order to more fully clarify the most severe grain refinement and the corresponding grain size, the microstructures in the topmost surface layers of the 3S Cu-Al alloys were carefully observed and the relevant TEM images for the microstructures of the 3S alloys with different Al contents and matrix grain sizes are shown in Fig. 6. The microstructure in the topmost surface layer of the Cu-5Al alloy with the A300 treatment consists of nanograins (NGs) with average grain sizes of the refined grains below 100 nm as shown in Fig. 6a1. The selected-area electron diffraction (SAED) inserted in Fig. 6a1 shows that the NGs are randomly oriented. For the Cu-5Al alloy with the A500 treatment as shown in Fig. 6a2, the grains are also refined to NGs and similar results are also realized in the Cu-5Al alloy with the A800 treatment as shown in Fig. 6a3. Moreover, the Cu-8Al alloy with the A300 treatment also exhibits refined NGs as shown in Fig. 6b1 and the microstructures in the topmost surface layer also consist of NGs in the Cu-8Al alloy with the A500 treatment as shown in Fig. 6b2 and in the Cu-8Al alloy with the A800 treatment as shown in Fig. 6b3. Similar results are obtained in Cu-11Al alloys, including the A300 treatment as shown in Fig. 6c1, the A500 treatment as shown in Fig. 6c2 and the A800 treatment as shown in Fig. 6c3. Therefore, it is concluded that the grains in the topmost surface layers for each group of Cu-Al alloys with different heat treatments are refined to NGs.

After the 3S treatment, the Cu-Al alloys with different Al contents and matrix grain sizes achieve gradient nanograined (GNG) structures. Besides the Cu-Al alloys treated by 3S in this work, some model and engineering metallic materials were also treated by different surface strengthening methods and yielded GNG structures. For example, a gradient-structured Ni was realized by rotationally accelerated shot peening (RASP) [28], a $\text{Cr}_{20}\text{Co}_{20}\text{Fe}_{20}\text{Ni}_{20}\text{Mn}_{20}$ high-entropy alloy (HEA) gave a gradient microstructure after an RASP treatment [6], a NiCoCr medium entropy alloy (MEA) gave a gradient nanolaminate microstructure after a shape-preserving machining treatment [4] a

Ti6Al4V alloy was surface nanocrystallized using an ultrasonic nano-crystal surface modification (UNSM) [29] and an AZ31 magnesium alloy gave a gradient structure by SMAT [30].

3.4. Microhardness distributions in the 3S Cu-Al alloys

One of the distinct gradient mechanical properties for surface-strengthened metallic materials is a gradient microhardness which is directly linked to the gradient microstructure. For example, an SMAT 304 stainless steel and Cu exhibited enhanced microhardness distributions with gradient characteristics [16, 25]. In this work, the effects of the Al content and matrix grain sizes on the microhardness distributions of the 3S Cu-Al were examined and the microhardness distributions in the surface layers with thicknesses of 2000 μm are shown in Fig. 7. The 3S Cu-5Al alloy with the A300 treatment has the maximum microhardness with a value of about 180 HV which is situated at the topmost surface layer but then the microhardness decreases rapidly along the depth direction as shown in Fig. 7a. The 3S Cu-8Al alloy with the A300 treatment has an enhanced maximum microhardness with a value of about 210 HV, and this maximum microhardness is located at the topmost surface layer. The microhardness decay rate is lower than for the Cu-5Al alloy with the A300 treatment as shown in Fig. 7a. The 3S Cu-11Al alloy with the A300 treatment has the highest maximum microhardness with a value of about 250 HV but the microhardness damping rate is similar to the Cu-5Al alloy with the A300 treatment as shown in Fig. 7a.

In addition, the three groups of Cu-Al alloys with the A400 treatment as shown in Fig. 7b and with the A500 treatment as shown in Fig. 7c have similar microhardness distributions by comparison with the Cu-Al alloys with the A300 treatment. From the Cu-5Al, Cu-8Al to Cu-11Al alloys, the maximum microhardness increases and the values are near to the results in Cu-Al alloys with the A300 treatment. The microhardness damping rates of the Cu-5Al and Cu-8Al alloys are approximate but the microhardness damping rate for the Cu-11Al alloy is a little faster than for the Cu-5Al alloys and Cu-8Al alloys. Moreover, the maximum microhardness in each group of Cu-Al alloys with the A600 treatment as shown in Fig. 7d, with the A700 treatment as

shown in Fig. 7e and with the A800 treatment as shown in Fig. 7f continue to increase with the increase of Al content, and the values of the maximum microhardness are similar to the Cu-Al alloys with the A300 treatment. However, the microhardness damping rates for the three groups of Cu-Al alloys under the A600 treatment, the A700 treatment, and the A800 treatment are approximate. Generally, the maximum microhardness for each group of Cu-Al alloys under the different heat treatments are stable, and therefore the microhardness distributions are complicated and dependent upon the changes in the Al contents and the matrix grain sizes.

4. Discussion

4.1. Characteristics of the maximum microhardness and thickness of the gradient layers in the 3S Cu-Al alloys

Usually the microstructure, residual stress and the microhardness in the gradient layer induced by surface mechanical strengthening exhibit major differences by comparison to the matrix. To better describe the gradient layer quantitatively, an exponential equation was established to relate the microhardness (H) distribution characteristic in the gradient layer together with the depth (d) direction as follows:

$$H = H_m + (H_M - H_m)e^{-Rd}, \quad (1)$$

where H_m , H_M , and R are the matrix microhardness, the maximum microhardness and the surface strengthening index of the gradient layer, respectively [21]. The thickness of the gradient layer (λ) is defined according to the depth in the microhardness-depth curve when the microhardness is near to H_m . Two major parameters are required to evaluate the mechanical properties of the gradient layer: the maximum microhardness and thickness of the gradient layer reveal the severe grain refinement in the topmost surface and the limit of plastic deformation in the depth direction, respectively.

Fig. 8 shows the effects of yield strength and work-hardening exponent of the matrices on the maximum microhardness of the 3S Cu-Al alloys with different Al contents and grain sizes. On the one hand, the 3S Cu-5Al alloy with different yield strengths determined by the grain sizes have an approximate maximum microhardness as shown in Fig. 8a and the 3S Cu-8Al and Cu-11Al alloys have similar variations

between the maximum microhardness and matrix strength. Therefore, the matrix strength is not the major factor influencing the maximum microhardness. On the other hand, the maximum microhardness remains stable with increasing work-hardening exponent for each group of the 3S Cu-Al alloys as shown in Fig. 8b. It is concluded that the level of grain refinement in the topmost surface layer is not related to the work-hardening exponent of the corresponding metallic materials. Therefore, the maximum microhardness induced by surface mechanical strengthening has less significance in the strength and work-hardening capability of the corresponding matrix.

Fig. 9 shows the variations of the thickness of the gradient layer in the 3S Cu-Al alloys with different Al contents and matrix grain sizes. When considering all 3S Cu-Al alloys uniformly, the thickness of the gradient layer decreases with increasing yield strength with a linear relation as shown in Fig. 9a. For high-strength metallic materials, it is difficult to obtain a thick gradient layer as in a CM400 maraging steel after a shot peening (SP) treatment and a 50CrMnMoVNb spring steel after the 3S treatment [13, 31]. Besides the matrix strength, the work-hardening exponent reveals the plastic deformation capacity which may influence the surface strengthening behavior, and the effect of the work-hardening exponent on the thickness of the gradient layer was examined as shown in Fig. 9b. For each group of the 3S Cu-Al alloys, the thickness of the gradient layer increases with an increase in the work-hardening exponent and metallic materials with high work-hardening exponents may be more easily surface-strengthened to give a thick gradient layer.

Therefore, the strength and work-hardening capacity are two major factors that cause a significant differences in the thicknesses of the gradient layers. In general, the matrix strength is a negative factor for the surface strengthening process and it effectively restrains any increase in thickness of the gradient layer. By contrast, the work-hardening exponent is a positive factor for the surface strengthening process and it promotes an external strain extending along the depth direction. During the surface mechanical strengthening process, this external stress is applied on the topmost surface layer as in the impact from the high-speed moving steel shots during the SP treatment and the grinding from high-speed rotating cutters during the 3S treatment in the present

work [32, 33]. Both the numerical measurements as in the finite element method and the experimental measurements as with X-rays reveal that the distribution of the applied plastic strain in the surface layer is graded [34-36]. Thus, the maximum plastic strain occurs at the topmost surface and then the plastic strain gradually decreases along the depth direction until it disappears. For the Cu-Al alloys with different Al contents and grain sizes, the applied plastic strain is sufficiently high to make the grains refined to become NGs in the topmost surface so that each group of the 3S Cu-Al alloy has similar values of the maximum microhardness. In addition, the plastic deformation of high-strength metallic materials is difficult but becomes easier for metallic materials with a high work-hardening capacity. As the applied plastic strain distribution is verified in this work, the low-strength or high work-hardening exponent Cu-Al alloys exhibit thick gradient layers.

4.2. Nature of the maximum microhardness of the gradient layer

As one of the important properties of the gradient layer, the maximum microhardness usually reveals the severest grain refinement and grain deformation at the topmost surface layer, and it further reflects the limitation of the plastic deformation induced by the surface mechanical strengthening. For example, a coarse-grained (CG) interstitial-free (IF) steel had the maximum microhardness with a value of about 2 GPa, and the original CGs with an average grain size of 26 μm were refined to NGs at the topmost nanostructured (NS) layer [37]. The microstructure at the maximum microhardness in the gradient layer mainly consisted of ultrafine and even nanoscale grains, dislocation cells and loose dislocations. After the surface mechanical strengthening, the microhardness was determined by the deformed microstructure at the topmost surface layer and the maximum microhardness was evaluated by the following equations:

$$H = a(\sigma_0 + M\alpha\mu b\sqrt{\rho} + \sigma_{\text{GB}}), \quad (2)$$

and

$$\sigma_{\text{GB}} = \frac{k_{\text{HP}}}{\sqrt{D}}, \quad (3)$$

where a is a constant to convert the flow stress to the measured hardness, σ_0 is the lattice friction stress, σ_{GB} is the contribution to the flow stress arising from the grain boundaries, k_{HP} is the Hall-Petch slope, D is the grain size and α , M , G , b and ρ are the Taylor constant, the Taylor factor, the shear modulus, the Burgers vector and the dislocation density, respectively [38-40]. As the 3S Cu-Al alloys have a similar microstructure at the topmost surface layer and the grains are also refined to a similar level, the maximum microhardness is related mainly to the Al content. For Cu-Al alloys, the values of σ_0 , ρ and σ_{GB} are affected by the Al content, especially σ_0 and σ_{GB} [22]. With an increase in the Al content, the solution strengthening effect is increased, the values of σ_0 and k_{HP} in σ_{GB} increase and the maximum microhardness also increases. In addition, the plastic deformation modes of Cu and Cu-Al alloys change from wavy slip to planar slip and twinning with increasing Al content and the corresponding decrease in the stacking fault energy (SFE), and Cu-Al alloys with high Al content and corresponding low SFE exhibit smaller grains when the severity of the external loading is enhanced [41, 42]. Under the same surface strengthening intensity as the 3S treatment in this work, the 3S Cu-11Al alloy may show NSGs with smaller grain sizes in the topmost surface layer than in the 3S Cu-5Al alloy, and the 3S Cu-8Al alloy will be intermediare as shown in Fig. 6. Combining the solution strengthening effect and the decrease in grain size, the maximum microhardness may be enhanced with the Al content.

In addition to the direct relation between the maximum microhardness and the Al content of 3S Cu-Al alloys, the plastic deformation of the surface-strengthened metals, including the grain deformation and grain refinement, is mainly determined by the applied stress as an external factor. During the surface mechanical process, the materials are treated by different surface strengthening methods under different external stresses, strain rates and temperatures, and the flow stress in the surface layer along the depth direction may be estimated using the modified Johnson-Cook (J-C) plasticity hardening model given by:

$$\sigma_f(d) = \left\{ \sigma_y(d) + B[\bar{\varepsilon}(d)]^n \right\} \left[1 + C \ln\left(\frac{\dot{\varepsilon}}{\dot{\varepsilon}_0}\right) \right] \left\{ 1 - \left[\frac{T(d) - T_r}{T_m - T_r} \right]^m \right\}, \quad (4)$$

where σ_y is the yield strength under the reference temperature (T_r), B , C , n , and m are

material constants, $\bar{\epsilon}$ is the equivalent strain, $\bar{\epsilon}_p$ is the normalized equivalent plastic strain by a reference strain rate where $\bar{\epsilon}_p$ is set to unity, T is the absolute temperature and T_m is the absolute melting temperature, respectively [36, 43]. According to Eq. (4), the flow stress distributions in the surface layer is related to the surface strengthening intensity, such as the spinning depth, the rotation speed and the moving speed which determines the 3S intensity. In addition, the plastic deformation during the surface mechanical strengthening process is also related to the characteristics of the metal as an internal factor, such as the deformation modes and the mechanical properties [33]. Therefore, it is necessary in this section to discuss both the external and internal factors on the maximum microhardness including for some metals treated by other surface strengthening methods [25, 28, 44-51], some metals treated by 3S in earlier studies [21, 33, 52] and the Cu-Al alloys treated by 3S in the present research.

Fig. 10 shows the maximum microhardness in the gradient layer for the surface strengthened metals and both the yield strength and work-hardening exponent are used to evaluate the variations of the maximum microhardness. As shown in Fig. 10a, low-strength metals exhibit a lower maximum microhardness, as in the AZ31 alloy and Cu treated by SMAT [25, 47]. With an increase in the yield strength of the as-received metal, the maximum microhardness increases as in pure Ti processed by a surface rolling treatment (SRT) and IN 718 alloy processed by SP [48, 51]. Furthermore, some metals with the same chemical compositions but different strengths have the same maximum microhardness after the surface strengthening, as in pure Cu [52] and in the Cu-Al alloys in this study [52].

Likewise, the effect of the work-hardening exponent on the maximum microhardness in the gradient layer of the different metals processed by different surface strengthening methods was also examined as shown in Fig. 10b. With a large range of work-hardening exponents, the maximum microhardness changes irregularly and the distributions of the maximum microhardness values are essentially random. Therefore, the maximum microhardness in the gradient layer is not directly connected with the plastic deformation capacity of the as-received metals.

From these results, it can be seen that the maximum microhardness of the surface strengthened metal is not related directly to the yield strength and work-hardening capacity of the as-received material and the essential factor affecting the maximum microhardness needs further investigation. In practice, Young's modulus describes the deformation resistance of the metal [53, 54] and the magnitude of Young's modulus is determined by the chemical composition of the metal less by the microstructure [55, 56]. As the maximum microhardness of the gradient layer of the 3S Cu-Al alloys increases with the Al content but is less related to the microstructure, it is reasonable to conclude that the maximum microhardness of the gradient layer is closely related to the value of Young's modulus. Accordingly, some surface-strengthened metals were selected to compare the differences introduced by Young's modulus in this work, including an AZ31 magnesium alloy processed by SMAT, severe shot peening (SSP) and SP [47, 57, 58], a 7075 aluminum alloy processed by SP and ultrasonic shot peening (USP) [59-61], a pure copper processed by SMAT, surface mechanical grinding treatment (SMGT) and 3S [25, 46, 52], an H62 copper alloy processed by 3S [33], a pure titanium processed by surface rolling treatment (STR) [51], a TC4 titanium alloy processed by laser peening (LP) and SP [62, 63], a 304 stainless steel processed by 3S and UIT [33, 64], a 316L stainless steel processed by RASP, SMAT and SSP [14, 49, 65], a 45 carbon steel processed by 3S [21] and an In718 superalloy processed by USP and SP [48, 66]. Using these data, the relation between the maximum microhardness of the gradient layer and the value of the Young's modulus in the corresponding as-received metal is shown in Fig. 11.

From Fig. 11, it is apparent that when the Young's modulus is low so the maximum microhardness is also low, as in Mg alloys, Cu alloys and Al alloys [25, 33, 46, 47, 52, 57-61]. With an increase in the Young's modulus, the maximum microhardness increases and the superalloy has the highest Young's modulus and the maximum microhardness [48, 66]. Some metals with approximately the same Young's modulus give different maximum microhardness after the surface mechanical strengthening [48, 62, 63, 66]. Nevertheless, the increased surface strengthening intensity is beneficial to the plastic deformation for obtaining smaller grains and an increased maximum

microhardness. For example, the LP TC4 alloy gives a higher maximum microhardness compared with the SP TC4 alloy [62, 63], and the USP In718 super alloy gives the higher maximum microhardness compared with the SP In718 super alloy [48, 66]. In addition, the plastic deformation mode changes with differences in the chemical compositions of the metals but the Young's modulus remains approximately the same with different chemical compositions. For example, the increased Al content in the Cu-Al alloys in this work enhances the solution strengthening effect and changes the plastic deformation mode, and the maximum microhardness increases with the increasing Al content under the same surface intensity for the 3S treatment. According to the relation between the Young's modulus and the maximum microhardness, it is concluded that Young's modulus may be considered as a fundamental parameter to evaluate the maximum microhardness. When the chemical compositions of metal are specified, both the Young's modulus and the plastic deformation mode may also be determined. As a result, the maximum microhardness of the surface-strengthened metals remains stable and it is determined primarily by the limitation of the grain refinement and grain deformation and it is less related to the microstructure of the as-received material.

4.3. Nature of the thickness of the gradient layer

During the surface mechanical strengthening process, the applied strain attenuates along the depth direction from the topmost surface to within the matrix. When the applied strain reaches a situation where it is insufficient to give plastic deformation so the corresponding depth may be regarded as the thickness of the gradient layer. Generally, it is easier in low-strength metals to obtain thicker gradient layers by comparison with high-strength metals. For example, AISI 316L stainless steel can produce a gradient layer with a thickness of about 800 μm after SMAT [65] while AISI 1045 steel only produces a gradient layer below 300 μm after the ball burnishing treatment [2].

However, the strength level is not the only factor influencing the thickness of the gradient layer. For pure Cu studied previously and the Cu-Al alloys in this work, it is difficult to obtain a thicker gradient layer in the cold-rolled samples with high strength

and low ductility but it becomes easier to obtain a thicker gradient layer in annealed samples with minor changes in strength and ductility [52]. Moreover, the plastic deformation capacity of the metal may be evaluated by the work-hardening stage in which the stress gradually increases with an increase in the plastic strain, and the work-hardening exponent may be regarded as a quantitative parameter to describe the plastic deformation capacity [67]. Concerning the plastic deformation during the surface mechanical strengthening, the gradient layer may be related to the work-hardening capacity of the corresponding as-received materials and the effects of strength and work-hardening capacity on the thickness of the gradient layer are now examined.

Fig. 12a shows the relation between the thickness of the gradient layer of the surface-strengthened metals and the yield strength of the corresponding as-received material where this also includes some metals treated by other different surface-strengthening methods from earlier reports [25, 28, 44-51], some metals treated by 3S in earlier studies [21, 33, 52, 68], and Cu-Al alloys treated by 3S in the present research. For the different metals treated by different surface-strengthening methods, the low-strength metals exhibit thick gradient layers, such as pure Cu processed by SMAT and CrCoNi MEA processed by NSRP [25, 44] and the Cu-Al alloys annealed at high temperatures in this work. With an increase in yield strength, the thickness of the gradient layer decreases as shown, for example by the 45 carbon steel processed earlier by 3S [21] and the Cu-Al alloys annealed at low temperatures in this work. Moreover, with a further increase in yield strength, the thickness of the gradient layer becomes very low. Therefore, it is concluded that the yield strength is an important factor restricting surface-strengthening and the strength may be regarded as an intrinsic factor affecting the thickness of the gradient layer.

Fig. 12b shows the relation between the thickness of the gradient layer of the surface-strengthened metals and the work-hardening exponent of the corresponding as-received materials. For metals with a low work-hardening exponent, the thickness of the gradient layer obtained by surface mechanical strengthening is very low as shown by the 50CrMnMoVNb steel processed earlier by 3S [13]. With an increase in the work-hardening exponent, the thickness of the gradient layer increases and the thickness of

the gradient layer is positive with the work-hardening exponent. Therefore, the thickness of the gradient layer increases exponentially with increasing work-hardening exponent and the work-hardening capacity may be a key factor in promoting the surface-strengthening effect.

Based on the effects of yield strength and work-hardening capacity on the thickness of the gradient layer, it appears that the thickness of the layer is determined by both the yield strength and work-hardening exponent, and in practice the yield strength is negative but the work-hardening exponent is positive for the thickness of the gradient layer. It follows therefore that, when constructing a gradient layer by surface mechanical strengthening, both the yield strength and work-hardening capacity should be considered. On the one hand, the main approaches to enhancing the yield strength are generally regulating the solute atoms by solid solution strengthening [69], precipitate particles by precipitation strengthening [70], dislocations by strain strengthening, and grain and twin boundaries by interfacial strengthening [71]. However, all of these strengthening phases are suppressive for the transportation of the applied strain in the gradient layer. On the other hand, the main approaches to enhancing the work-hardening capacity are increasing the grain size and the percentage of ductile phases [72], decreasing the stacking fault energy (SFE), and changing the plastic deformation mode from wavy to planar slip [41]. All of these approaches can promote plastic deformation during the surface mechanical strengthening and, as a result, the thickness of the gradient layer increases with a decrease in yield strength and an increase in the work-hardening exponent which is mainly related to the microstructure and less related to the chemical composition.

4.4. Proposals for improving the properties of the gradient layer

The overall objective of surface mechanical strengthening is to improve the service performance of metallic materials and the core of this approach is the construction of a gradient layer with enhanced microhardness and extended thickness. According to the effect of the Al content and grain size on the properties of the gradient layer in the 3S Cu-Al alloys used in this work, the three factors of composition, microstructure and

strengthening method may be examined separately in order to summarize the optimum procedure for improving the properties of the gradient layer in surface-strengthened metals. These factors are examined in the following sub-sections.

i) **Composition.** When preparing the metallic materials, the first principle is to select the chemical composition. Both the Young's modulus and the plastic deformation mode are related to the composition of the metal. After the surface mechanical strengthening, metals with two different compositions have different hardness-depth ($H-d$) curves as shown in Fig. 13a1, and the maximum microhardness is less related to the mechanical properties when the composition of the metal is given as shown in Fig. 13a2. With the increase of Young's modulus in the as-received metal, the maximum microhardness may increase, and the plastic deformation mode also affects the maximum microhardness when Young's modulus is approximately the same as shown in Fig. 13a3. Therefore, it is concluded that after surface mechanical strengthening the maximum microhardness of the gradient layer remains stable when the chemical compositions are known and it is less related to the microstructure of the as-received metal.

ii) **Microstructure.** For as-received metals, both yield strength and work-hardening capacity are closely related to the microstructure. For example, the grain sizes of the Cu-Al alloys increase with increasing annealing temperature and the yield strength decreases and the work-hardening exponent increases. As shown in Fig. 13b1, the microstructure distribution and $H-d$ curve in the surface layer of the surface-strengthened metal vary with the change in microstructure of the as-received metal, and metals with enhanced strength due to changeable compositions may exhibit increased microhardness distributions and maximum microhardness in the gradient layer. With an increase in yield strength in the as-received metal, the thickness of the gradient layer of the surface-strengthened metal decreases as shown in Fig. 13b2. In addition, with an increase in the work-hardening exponent of the as-received metal, the thickness of the gradient layer of the surface-strengthened material increases as shown in Fig. 13b3. Thus, it is concluded that after the surface mechanical strengthening the thickness of the gradient layer is closely related the microstructure of the as-received metal and it is

less related to the composition of the material.

iii) **Strengthening method.** Over the last two decades, some practical surface mechanical techniques were designed to improve the properties of the gradient layer. In terms of the traditional SP treatment, rotationally accelerated shot peening with a higher surface strengthening intensity was developed and the RASP Cu and 316L stainless steel exhibited gradient nanostructures (GNSs) with higher maximum microhardness and thicker gradient layer [49, 73]. Also, severe shot peening (SSP) with a higher surface strengthening intensity was developed and the SSP AISI 1017 mild steel showed improved properties in the gradient layer [74]. The external increase of surface strengthening intensity (SSI) may indeed improve the microhardness as illustrated in Fig. 13c1. With an increase in SSI, both the maximum microhardness and the thickness of the gradient layer increases as shown in Fig. 13c1 and Fig. 13c2, respectively.

Based on these results and conclusions, it is possible to now present some specific proposals for improving the properties of the gradient layer of metallic materials. These proposals are summarized schematically in Fig. 14.

The first proposal is to design the composition. During the surface mechanical strengthening in this research, the maximum microhardness of the gradient layer remained stable without a change of chemical composition and it became adjustable with changing chemical compositions. By designing a reasonable composition, the metal is strengthened by solid solution atoms and precipitate particles and also plastic deformation may be easier.

The second proposal is to optimize the microstructure. Generally, the mechanical properties of metals may be optimized by microstructural optimization, such as by improving the strength and decreasing the ductility through an increase in grain size. Correspondingly, the thickness of the gradient layer may be increased after the surface mechanical strengthening by optimizing the microstructure of the metal to achieve a suitable strength and work-hardening capacity.

The third proposal is to improve the surface strengthening intensity. From traditional shot peening to laser peening and ultrasonic shot peening, and even the novel

surface mechanical rolling treatment (SMRT) and surface spinning strengthening [61, 75], are now available as surface strengthening technologies which incorporate enhanced surface strengthening intensities.

In general, a compositional design, microstructural optimization and an adaptation of appropriate surface strengthening technology should be considered during the surface strengthening. Thus, enhanced properties of the gradient layer, such as an increased maximum microhardness and extended thickness, may be realized by optimizing the chemical compositions and microstructures of the metals and by selecting the optimum surface strengthening technology.

5. Summary and conclusions

Cu-Al alloys with different Al contents and grain sizes were treated by surface spinning strengthening (3S) and the properties of the gradient layer, including the maximum microhardness and thickness, were then examined. The following conclusions summarize the main results from these experiments:

i) Each group of the 3S Cu-Al alloys had approximately the same maximum microhardness in the gradient layers and this maximum microhardness increased with an increase in the Al content. An essential relationship was established between the maximum microhardness and chemical composition which delineates the Young's modulus and plastic deformation mode of the metal, and the maximum microhardness of the gradient layer was enhanced with an increase in the Young's modulus.

ii) The thickness of the gradient layer in the 3S Cu-Al alloys increased with a decrease in the yield strength and an increase in the work-hardening exponent, respectively. An essential relationship was established between the thickness of the gradient layer and the microstructure which determines the strength and work-hardening capacity of metals. It was found that the strength restricts but the work-hardening capacity promotes an increase in the thickness of the gradient layer, respectively.

iii) The maximum microhardness of the gradient layer depends primarily on the chemical composition and the corresponding Young's modulus and plastic deformation

mode with much less dependence on the microstructure and mechanical properties. The thickness of the gradient layer depends mainly depend on the strength and work-hardening capacity which is closely related to the microstructure. By combining the compositional design and a microstructural optimization of the as-received metal, and by improving the surface strengthening intensity, it is possible to attain a gradient layer of the surface-strengthened metal with an enhanced maximum microhardness and extended thickness.

Acknowledgements

This work was supported by the National Natural Science Foundation of China (NSFC) under grant No. U1664253, Lu Jiayi International Team Project and Liaoning Revitalization Talents Program under grant No. XLYC1808027. One of the authors was supported by the European Research Council under grant agreement no. 267464-SPDMETALS (TGL).

References

- [1] M. Yasuoka, P. Wang, K. Zhang, Z. Qiu, K. Kusaka, Y.S. Pyoun, R.I. Murakami, Improvement of the fatigue strength of SUS304 austenite stainless steel using ultrasonic nanocrystal surface modification, *Surf. Coat. Technol.* 218 (2013) 93-98.
- [2] R. Avilés, J. Albizuri, A. Rodríguez, L.N. López de Lacalle, Influence of low-plasticity ball burnishing on the high-cycle fatigue strength of medium carbon AISI 1045 steel, *Int. J. Fatigue* 55 (2013) 230-244.
- [3] C.W. Shao, P. Zhang, Y.K. Zhu, Z.J. Zhang, J.C. Pang, Z.F. Zhang, Improvement of low-cycle fatigue resistance in TWIP steel by regulating the grain size and distribution, *Acta Mater.* 134 (2017) 128-142.
- [4] W. Guo, Z. Pei, X. Sang, J.D. Poplawsky, S. Bruschi, J. Qu, D. Raabe, H. Bei, Shape-preserving machining produces gradient nanolaminate medium entropy alloys with high strain hardening capability, *Acta Mater.* 170 (2019) 176-186.
- [5] Z. Cheng, H. Zhou, Q. Lu, H. Gao, L. Lu, Extra strengthening and work hardening in gradient nanotwinned metals, *Science* 362 (2018) eaau1925.
- [6] M.N. Hasan, Y.F. Liu, X.H. An, J. Gu, M. Song, Y. Cao, Y.S. Li, Y.T. Zhu, X.Z. Liao,

- Simultaneously enhancing strength and ductility of a high-entropy alloy via gradient hierarchical microstructures, *Int. J. Plast.* 123 (2019) 178-195.
- [7] Z. Zeng, X. Li, D. Xu, L. Lu, H. Gao, T. Zhu, Gradient plasticity in gradient nano-grained metals, *Extr. Mech. Lett.* 8 (2016) 213-219.
- [8] A.Y. Chen, J.B. Liu, H.T. Wang, J. Lu, Y.M. Wang, Gradient twinned 304 stainless steels for high strength and high ductility, *Mater. Sci. Eng. A* 667 (2016) 179-188.
- [9] K. Ito, T. Okuda, R. Ueji, H. Fujii, C. Shiga, Increase of bending fatigue resistance for tungsten inert gas welded SS400 steel plates using friction stir processing, *Mater. Des.* 61 (2014) 275-280.
- [10] L.L. Zhu, H.H. Ruan, A.Y. Chen, X. Guo, J. Lu, Microstructures-based constitutive analysis for mechanical properties of gradient-nanostructured 304 stainless steels, *Acta Mater.* 128 (2017) 375-390.
- [11] D.A. Lesyk, S. Martinez, B.N. Mordyuk, V.V. Dzhemelinskyi, A. Lamikiz, G.I. Prokopenko, K.E. Grinkevych, I.V. Tkachenko, Laser-hardened and ultrasonically peened surface layers on tool steel AISI D2: correlation of the bearing curves' parameters, hardness and wear, *J. Mater. Eng. Perform.* 27 (2017) 764-776.
- [12] X. Yan, S. Yin, C. Chen, R. Jenkins, R. Lupoi, R. Bolot, W. Ma, M. Kuang, H. Liao, J. Lu, M. Liu, Fatigue strength improvement of selective laser melted Ti6Al4V using ultrasonic surface mechanical attrition, *Mater. Res. Lett.* 7 (2019) 327-333.
- [13] C.X. Ren, D.Q.Q. Wang, Q. Wang, Y.S. Guo, Z.J. Zhang, C.W. Shao, H.J. Yang, Z.F. Zhang, Enhanced bending fatigue resistance of a 50CrMnMoVNb spring steel with decarburized layer by surface spinning strengthening, *Int. J. Fatigue* 124 (2019) 277-287.
- [14] S. Bagherifard, S. Slawik, I. Fernández-Pariente, C. Pauly, F. Mücklich, M. Guagliano, Nanoscale surface modification of AISI 316L stainless steel by severe shot peening, *Mater. Des.* 102 (2016) 68-77.
- [15] J. Li, S. Chen, X. Wu, A.K. Soh, A physical model revealing strong strain hardening in nano-grained metals induced by grain size gradient structure, *Mater. Sci. Eng. A* 620 (2015) 16-21.

- [16] X.L. Wu, M.X. Yang, F.P. Yuan, L. Chen, Y.T. Zhu, Combining gradient structure and TRIP effect to produce austenite stainless steel with high strength and ductility, *Acta Mater.* 112 (2016) 337-346.
- [17] S.Q. Deng, A. Godfrey, W. Liu, N. Hansen, A gradient nanostructure generated in pure copper by platen friction sliding deformation, *Scr. Mater.* 117 (2016) 41-45.
- [18] J. Li, Q. Mei, Y. Li, B. Wang, Production of surface layer with gradient microstructure and microhardness on copper by high pressure surface rolling, *Metals* 10 (2020) 73.
- [19] U. Martin, I. Altenberger, B. Scholtes, K. Kremmer, H. Oettel, Cyclic deformation and near surface microstructures of normalized shot peened steel SAE 1045, *Mater. Sci. Eng. A* 246 (1998) 69-80.
- [20] R.F. Kubler, S. Berveiller, D. Bouscaud, R. Guiheux, E. Patoor, Q. Puydt, Shot peening of TRIP780 steel: Experimental analysis and numerical simulation, *J. Mater. Process. Technol.* 270 (2019) 182-194.
- [21] C.X. Ren, Q. Wang, Z.J. Zhang, P. Zhang, Z.F. Zhang, Surface strengthening behaviors of four structural steels processed by surface spinning strengthening, *Mater. Sci. Eng. A* 704 (2017) 262-273.
- [22] C.X. Ren, Q. Wang, J.P. Hou, Z.J. Zhang, H.J. Yang, Z.F. Zhang, Exploring the strength and ductility improvement of Cu-Al alloys, *Mater. Sci. Eng. A* 786 (2020) 139441.
- [23] Y.Z. Tian, Y. Bai, L.J. Zhao, S. Gao, H.K. Yang, A. Shibata, Z.F. Zhang, N. Tsuji, A novel ultrafine-grained Fe-22Mn-0.6C TWIP steel with superior strength and ductility, *Mater. Charact.* 126 (2017) 74-80.
- [24] S.J. Sun, Y.Z. Tian, H.R. Lin, X.G. Dong, Y.H. Wang, Z.J. Zhang, Z.F. Zhang, Enhanced strength and ductility of bulk CoCrFeMnNi high entropy alloy having fully recrystallized ultrafine-grained structure, *Mater. Des.* 133 (2017) 122-127.
- [25] S. Shahrezaei, Y. Sun, S.N. Mathaudhu, Strength-ductility modulation via surface severe plastic deformation and annealing, *Mater. Sci. Eng. A* 761 (2019) 138023.
- [26] Y. Bai, Y. Momotani, M.C. Chen, A. Shibata, N. Tsuji, Effect of grain refinement on hydrogen embrittlement behaviors of high-Mn TWIP steel, *Mater. Sci. Eng. A*

651 (2016) 935-944.

- [27] H.K. Yang, Y.Z. Tian, Z.J. Zhang, Z.F. Zhang, Simultaneously improving the strength and ductility of Fe-22Mn-0.6C twinning-induced plasticity steel via nitrogen addition, *Mater. Sci. Eng. A* 715 (2018) 276-280.
- [28] Y.F. Wang, C.X. Huang, Y.S. Li, F.J. Guo, Q. He, M.S. Wang, X.L. Wu, R.O. Scattergood, Y.T. Zhu, Dense dispersed shear bands in gradient-structured Ni, *Int. J. Plast.* 124 (2020) 186-198.
- [29] J. Liu, S. Suslov, A. Vellore, Z. Ren, A. Amanov, Y.-S. Pyun, A. Martini, Y. Dong, C. Ye, Surface nanocrystallization by ultrasonic nano-crystal surface modification and its effect on gas nitriding of Ti6Al4V alloy, *Mater. Sci. Eng. A* 736 (2018) 335-343.
- [30] X. Yan, X. Meng, L. Luo, Y. Jing, G. Yi, J. Lu, Y. Liu, Mechanical behaviour of AZ31 magnesium alloy with the laminate and gradient structure, *Philos. Mag.* 99 (2019) 3059-3077.
- [31] Q.Q. Duan, B. Wang, P. Zhang, K. Yang, Z.F. Zhang, Improvement of notch fatigue properties of ultra-high CM400 maraging steel through shot peening, *J. Mater. Res.* 32 (2017) 4424-4432.
- [32] B.N. Mordyuk, Y.V. Milman, M.O. Iefimov, G.I. Prokopenko, V.V. Silberschmidt, M.I. Danylenko, A.V. Kotko, Characterization of ultrasonically peened and laser-shock peened surface layers of AISI 321 stainless steel, *Surf. Coat. Technol.* 202 (2008) 4875-4883.
- [33] C.X. Ren, Q. Wang, Z.J. Zhang, H.J. Yang, Z.F. Zhang, Enhanced tensile and bending yield strengths of 304 stainless steel and H62 brass by surface spinning strengthening, *Mater. Sci. Eng. A* 754 (2019) 593-601.
- [34] M. Ayeb, M. Frija, R. Fathallah, Prediction of residual stress profile and optimization of surface conditions induced by laser shock peening process using artificial neural networks, *Int. J. Adv. Manuf. Technol.* 100 (2018) 2455-2471.
- [35] M. Klemenz, V. Schulze, O. Vöhringer, D. Löhe, Finite Element Simulation of the Residual Stress States after Shot Peening, *Mater. Sci. Forum* 524-525 (2006) 349-354.

- [36] S.C. Cao, X.C. Zhang, J. Lu, Y.L. Wang, S.Q. Shi, R.O. Ritchie, Predicting surface deformation during mechanical attrition of metallic alloys, *npj Comput. Mater.* 5 (2019) 36.
- [37] F. Yuan, D. Yan, J. Sun, L. Zhou, Y. Zhu, X. Wu, Ductility by shear band delocalization in the nano-layer of gradient structure, *Mater. Res. Lett.* 7 (2018) 12-17.
- [38] P. Zhang, S.X. Li, Z.F. Zhang, General relationship between strength and hardness, *Mater. Sci. Eng. A* 529 (2011) 62-73.
- [39] J. Li, A.K. Soh, Modeling of the plastic deformation of nanostructured materials with grain size gradient, *Int. J. Plast.* 39 (2012) 88-102.
- [40] Z. Yanushkevich, S.V. Dobatkin, A. Belyakov, R. Kaibyshev, Hall-Petch relationship for austenitic stainless steels processed by large strain warm rolling, *Acta Mater.* 136 (2017) 39-48.
- [41] R. Liu, Z.J. Zhang, L.L. Li, X.H. An, Z.F. Zhang, Microscopic mechanisms contributing to the synchronous improvement of strength and plasticity (SISP) for TWIP copper alloys, *Sci. Rep.* 5 (2015) 9550.
- [42] X.H. An, Q.Y. Lin, S.D. Wu, Z.F. Zhang, R.B. Figueiredo, N. Gao, T.G. Langdon, Significance of stacking fault energy on microstructural evolution in Cu and Cu-Al alloys processed by high-pressure torsion, *Philos. Mag.* 91 (2011) 3307-3326.
- [43] A. He, G. Xie, H. Zhang, X. Wang, A comparative study on Johnson-Cook, modified Johnson-Cook and Arrhenius-type constitutive models to predict the high temperature flow stress in 20CrMo alloy steel, *Mater. Des.* 52 (2013) 677-685.
- [44] R. Wen, C. You, L. Zeng, H. Wang, X. Zhang, Achieving a unique combination of strength and ductility in CrCoNi medium-entropy alloy via heterogeneous gradient structure, *J. Mater. Sci.* 55 (2020) 12544-12553.
- [45] M.X. Yang, R.G. Li, P. Jiang, F.P. Yuan, Y.D. Wang, Y.T. Zhu, X.L. Wu, Residual stress provides significant strengthening and ductility in gradient structured materials, *Mater. Res. Lett.* 7 (2019) 433-438.
- [46] J. Long, Q. Pan, N. Tao, M. Dao, S. Suresh, L. Lu, Improved fatigue resistance of gradient nanograined Cu, *Acta Mater.* 166 (2019) 56-66.

- [47] L. Chen, F. Yuan, P. Jiang, J. Xie, X. Wu, Mechanical properties and deformation mechanism of Mg-Al-Zn alloy with gradient microstructure in grain size and orientation, *Mater. Sci. Eng. A* 694 (2017) 98-109.
- [48] W. Zeng, J. Yang, Quantitative representation of mechanical behavior of the surface hardening layer in shot-peened nickel-based superalloy, *Materials* 13 (2020) 1437.
- [49] J.S. Li, W.D. Gao, Y. Cao, Z.W. Huang, B. Gao, Q.Z. Mao, Y.S. Li, Microstructures and mechanical properties of a gradient nanostructured 316L stainless steel processed by rotationally accelerated shot peening, *Adv. Eng. Mater.* 20 (2018) 1800402.
- [50] W. Zhou, X. Ren, Y. Yang, Z. Tong, L. Chen, Tensile behavior of nickel with gradient microstructure produced by laser shock peening, *Mater. Sci. Eng. A* 771 (2020) 138603.
- [51] Q. Wang, J. Ren, Y. Wang, C. Xin, L. Xiao, D. Yang, Deformation and fracture mechanisms of gradient nanograined pure Ti produced by a surface rolling treatment, *Mater. Sci. Eng. A* 754 (2019) 121-128.
- [52] C.X. Ren, Q. Wang, Z.J. Zhang, H.J. Yang, Z.F. Zhang, Surface strengthening behaviors of pure Cu with heterogeneous microstructures, *Mater. Sci. Eng. A* 727 (2018) 192-199.
- [53] J.D. Giallonardo, U. Erb, K.T. Aust, G. Palumbo, The influence of grain size and texture on the Young's modulus of nanocrystalline nickel and nickel-iron alloys, *Philos. Mag.* 91 (2011) 4594-4605.
- [54] S. Fahy, J. O'Riordan, C. O'Sullivan, P. Twomey, How reflected wave fronts dynamically establish Hooke's law in a spring, *Eur. J. Phys.* 33 (2012) 417-426.
- [55] H. Matsumoto, S. Watanabe, N. Masahashi, S. Hanada, Composition dependence of Young's modulus in Ti-V, Ti-Nb, and Ti-V-Sn alloys, *Metall. Mater. Trans. A* 37A (2006) 3239-3249.
- [56] J. Chen, L. Zhang, Composition-dependent hardness and Young's modulus in fcc Ni-X (X = Rh, Ta, W, Re, Os, and Ir) alloys: Experimental measurements and CALPHAD modeling, *J. Mater. Res.* 34 (2019) 3104-3115.

- [57] S. Bagherifard, D.J. Hickey, S. Fintova, F. Pastorek, I. Fernandez-Pariente, M. Bandini, T.J. Webster, M. Guagliano, Effects of nanofeatures induced by severe shot peening (SSP) on mechanical, corrosion and cytocompatibility properties of magnesium alloy AZ31, *Acta Biomater.* 66 (2018) 93-108.
- [58] M. Jamalain, D.P. Field, Effect of gradient microstructures on strengthening and toughening of AZ31, *Mater. Sci. Eng. A* 771 (2020) 138615.
- [59] U. Zupanc, J. Grum, Surface integrity of shot peened aluminium alloy 7075-T651, *Stroj Vestn-Int. J. Mech. Eng.* 57 (2011) 379-384.
- [60] M. Benedetti, V. Fontanari, P. Scardi, C.L.A. Ricardo, M. Bandini, Reverse bending fatigue of shot peened 7075-T651 aluminium alloy: The role of residual stress relaxation, *Int. J. Fatigue* 31 (2009) 1225-1236.
- [61] V. Pandey, K. Chattopadhyay, N.C. Santhi Srinivas, V. Singh, Role of ultrasonic shot peening on low cycle fatigue behavior of 7075 aluminium alloy, *Int. J. Fatigue* 103 (2017) 426-435.
- [62] S. Huang, E. Agyenim-Boateng, J. Sheng, G. Yuan, F.Z. Dai, D.H. Ma, J.X. Zhao, J.Z. Zhou, Effects of laser peening with different laser power densities on the mechanical properties of hydrogenated TC4 titanium alloy, *Int. J. Hydrogen Energy* 44 (2019) 17114-17126.
- [63] Y.G. Liu, M.Q. Li, H.J. Liu, Surface nanocrystallization and gradient structure developed in the bulk TC4 alloy processed by shot peening, *J. Alloys Compd.* 685 (2016) 186-193.
- [64] D.A. Lesyk, H. Soyama, B.N. Mordyuk, V.V. Dzhemelinskyi, S. Martinez, N.I. Khripta, A. Lamikiz, Mechanical surface treatments of AISI 304 stainless steel: Effects on surface microrelief, residual stress, and microstructure, *J. Mater. Eng. Perform.* 28 (2019) 5307-5322.
- [65] B. Arifvianto, Suyitno, M. Mahardika, P. Dewo, P.T. Iswanto, U.A. Salim, Effect of surface mechanical attrition treatment (SMAT) on microhardness, surface roughness and wettability of AISI 316L, *Mater. Chem. Phys.* 125 (2011) 418-426.
- [66] S. Kumar, G. Sudhakar Rao, K. Chattopadhyay, G.S. Mahobia, N.C. Santhi Srinivas, V. Singh, Effect of surface nanostructure on tensile behavior of superalloy

- IN718, *Mater. Des.* 62 (2014) 76-82.
- [67] M. Naghizadeh, H. Mirzadeh, Effects of grain size on mechanical properties and work-hardening behavior of AISI 304 austenitic stainless steel, *Steel Res. Int.* 90 (2019) 1900153.
- [68] C.X. Ren, Q. Wang, J.P. Hou, Z.J. Zhang, H.J. Yang, Z.F. Zhang, Revealing the maximum microhardness and thickness of hardened layers for copper with various grain sizes, *Mater. Sci. Eng. A* 778 (2020) 139113.
- [69] J.A. Yasi, L.G. Hector, D.R. Trinkle, First-principles data for solid-solution strengthening of magnesium: From geometry and chemistry to properties, *Acta Mater.* 58 (2010) 5704-5713.
- [70] P. Hidalgo-Manrique, J.D. Robson, M.T. Pérez-Prado, Precipitation strengthening and reversed yield stress asymmetry in Mg alloys containing rare-earth elements: A quantitative study, *Acta Mater.* 124 (2017) 456-467.
- [71] Q. Lai, P. Song, H. Zhou, L. Xiao, T. Feng, C. Li, Deformation-induced martensitic transformation and strain hardening in a nanocrystalline FeMn alloy processed by severe austenite pre-deformation, *Materialia* 13 (2020) 100832.
- [72] J. Zhang, S. Hao, D. Jiang, Y. Huan, L. Cui, Y. Liu, H. Yang, Y. Ren, In situ synchrotron high-energy X-ray diffraction study of microscopic deformation behavior of a hard-soft dual phase composite containing phase transforming matrix, *Acta Mater.* 130 (2017) 297-309.
- [73] X. Wang, Y.S. Li, Q. Zhang, Y.H. Zhao, Y.T. Zhu, Gradient structured copper by rotationally accelerated shot peening, *J. Mater. Sci. Technol.* 33 (2017) 758-761.
- [74] O. Unal, R. Varol, Almen intensity effect on microstructure and mechanical properties of low carbon steel subjected to severe shot peening, *Appl. Surf. Sci.* 290 (2014) 40-47.
- [75] C. Xin, Q. Sun, L. Xiao, J. Sun, Biaxial fatigue property enhancement of gradient ultra-fine-grained Zircaloy-4 prepared by surface mechanical rolling treatment, *J. Mater. Sci.* 53 (2018) 12492-12503.

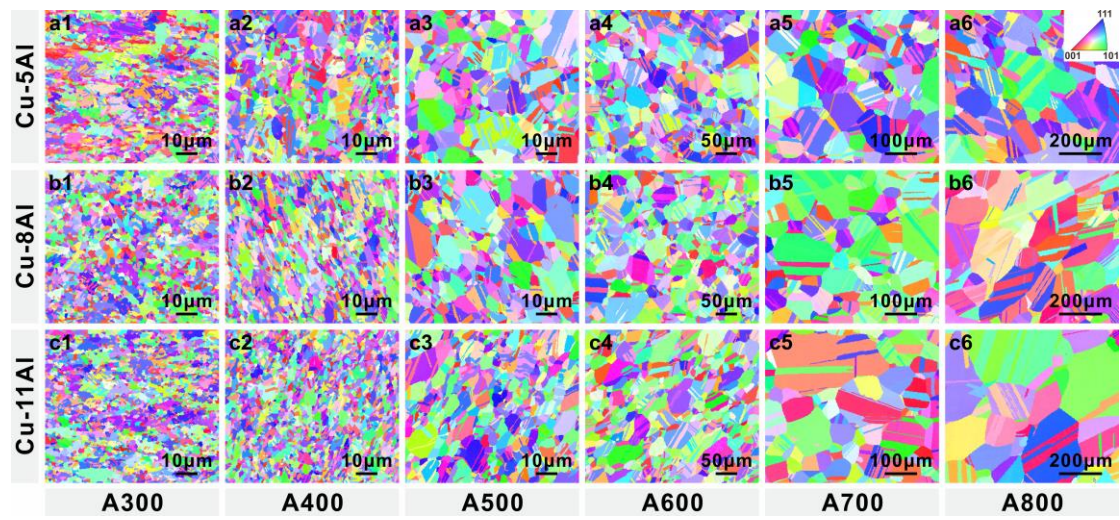


Fig. 1. Microstructures of the Cu-Al alloys with different Al contents and grain sizes characterized by SEM-EBSD. (a1-a6) Cu-5Al alloys; (b1-b6) Cu-8Al alloys; (c1-c6) Cu-11Al alloys.

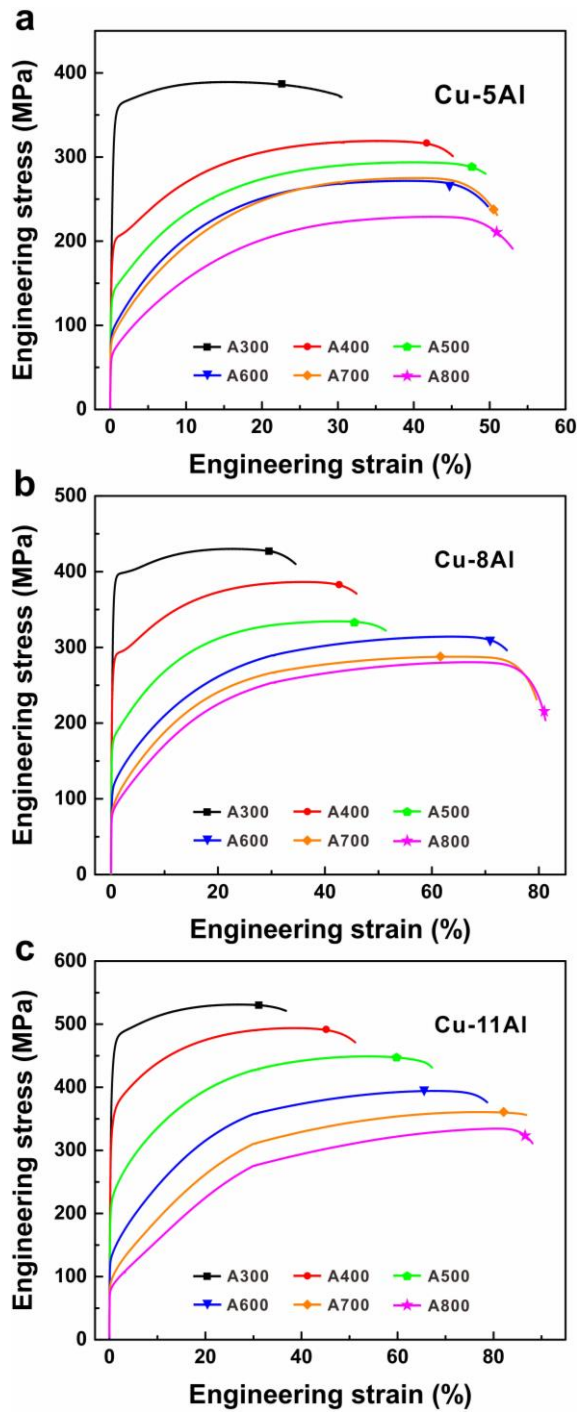


Fig. 2. Tensile engineering stress-strain curves of the as-received Cu-Al alloys with different Al contents and grain sizes. (a) Cu-5Al alloy; (b) Cu-8Al alloy; (c) Cu-11Al alloy [22].

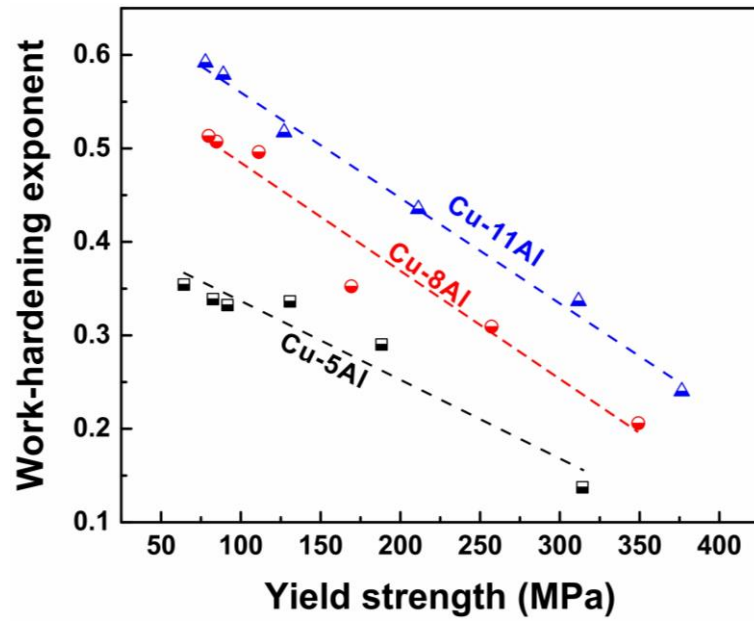


Fig. 3. Variations between the work-hardening exponent and yield strength of the as-received Cu-Al alloys with different Al contents and grain sizes.

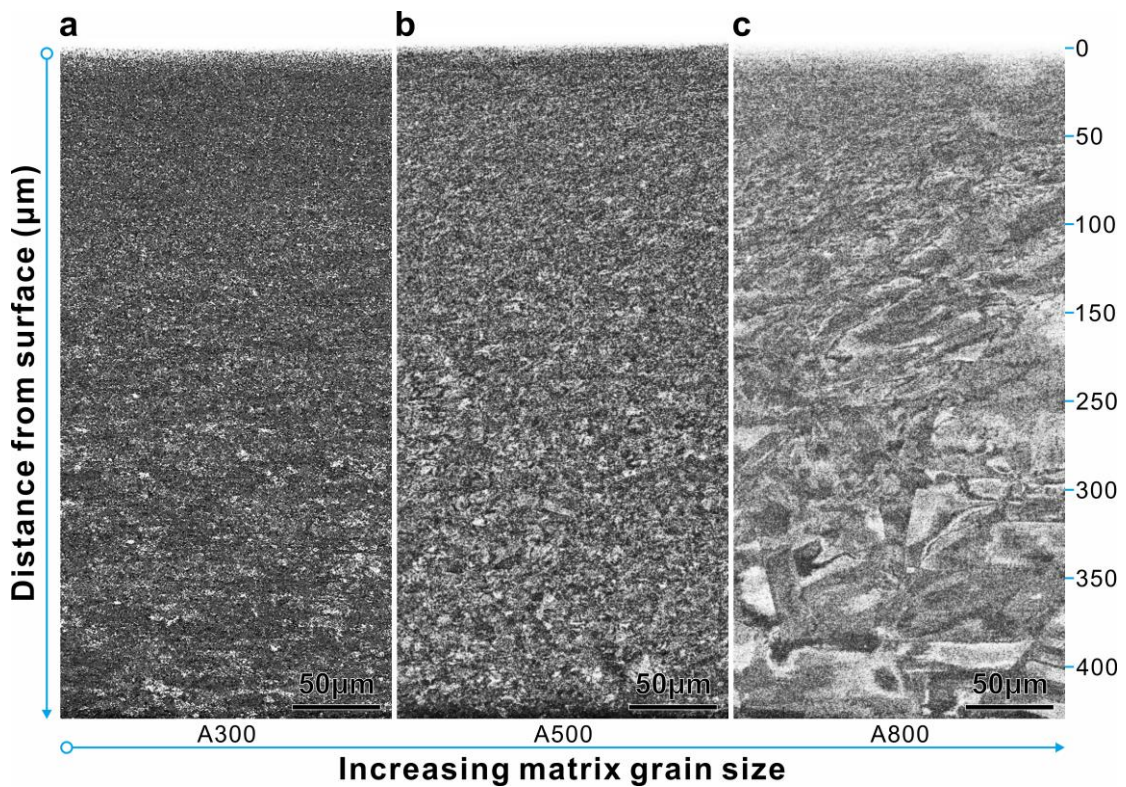


Fig. 4. SEM-ECC images of gradient microstructures for the 3Sed Cu-5Al alloys with the different matrix grain sizes induced by different heat treatments. (a) A300 treatment; (b) A500 treatment; (c) A800 treatment.

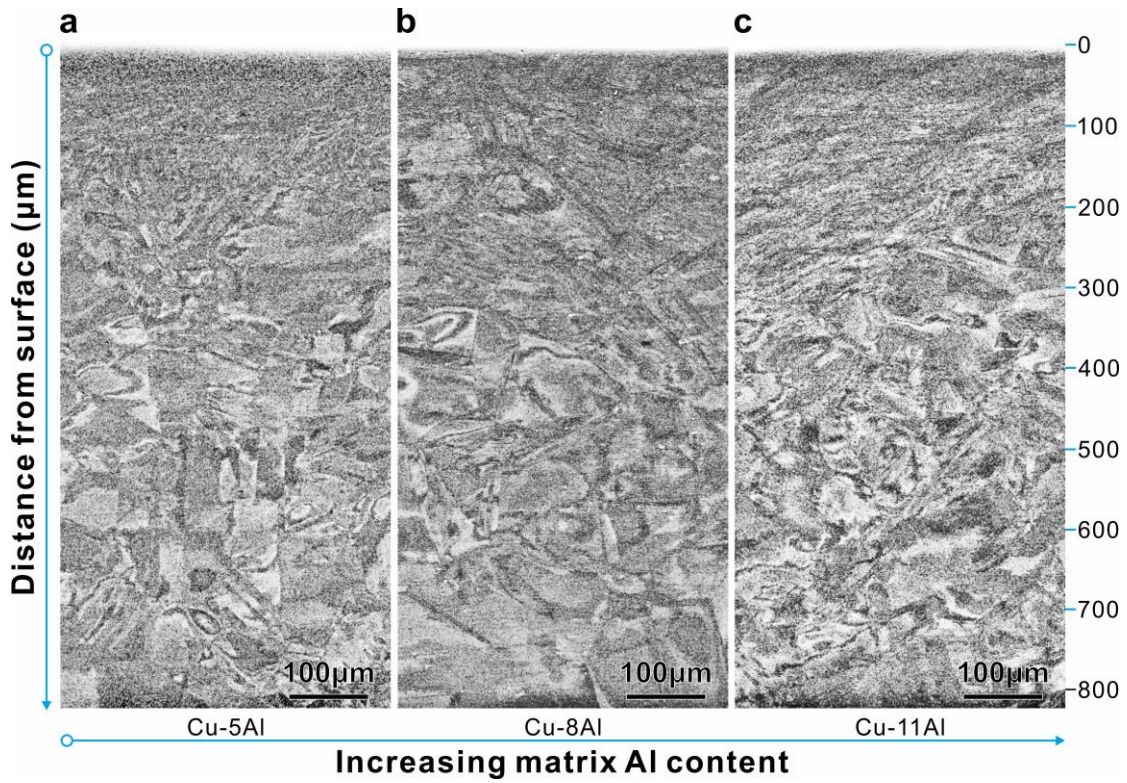


Fig. 5. SEM-ECC images of gradient microstructures for the 3Sed Cu-Al alloys with the A800 treatment. (a) Cu-5Al alloy; (b) Cu-8Al alloy; (c) Cu-11Al alloy.

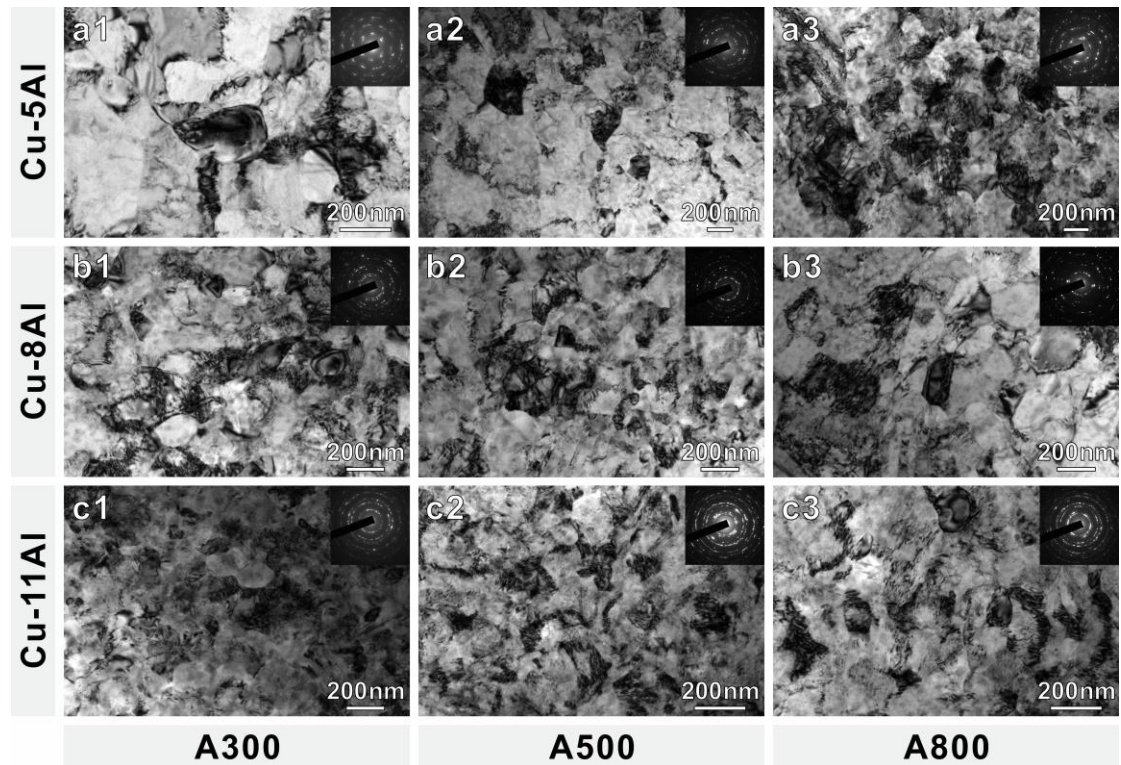


Fig. 6. TEM images of microstructures in the topmost surface layers (about 25 μm to the topmost surface) for the 3Sed Cu-Al alloys with different Al contents and matrix

grain sizes. (a1) Cu-5Al alloy with A300 treatment; (a2) Cu-5Al alloy with A500 treatment; (a3) Cu-5Al alloy with A800 treatment; (b1) Cu-8Al alloy with A300 treatment; (b2) Cu-8Al alloy with A500 treatment; (b3) Cu-5Al alloy with A800 treatment; (c1) Cu-11Al alloy with A300 treatment; (c2) Cu-11Al alloy with A500 treatment; (c3) Cu-11Al alloy with A800 treatment.

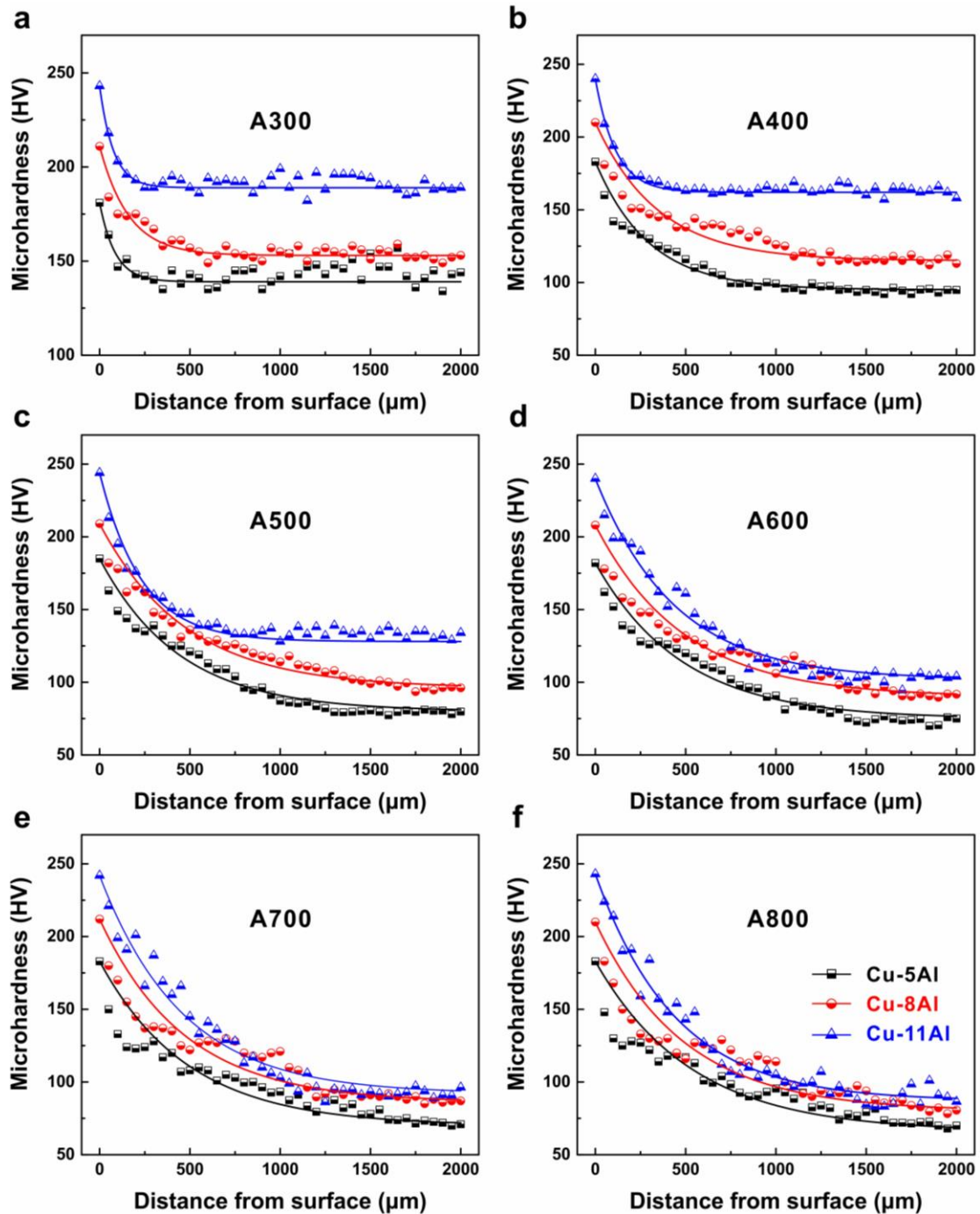


Fig. 7. Microhardness distributions in the surface layer with the thickness of 2000 μm

for the 3Sed Cu-Al alloys with different Al contents and grain sizes. (a) A300 treatment; (b) A400 treatment; (c) A500 treatment; (d) A600 treatment; (e) A700 treatment; (f) A800 treatment.

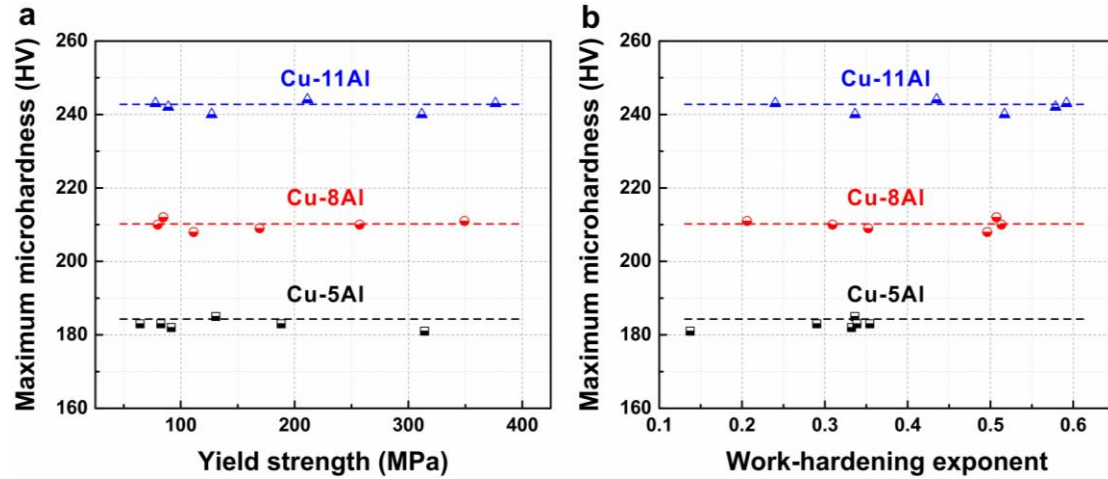


Fig. 8. The maximum microhardness of the 3Sed Cu-Al alloys with different Al contents and matrix grain sizes. (a) Relation between the maximum microhardness and yield strength; (b) relation between the maximum microhardness and work-hardening exponent.

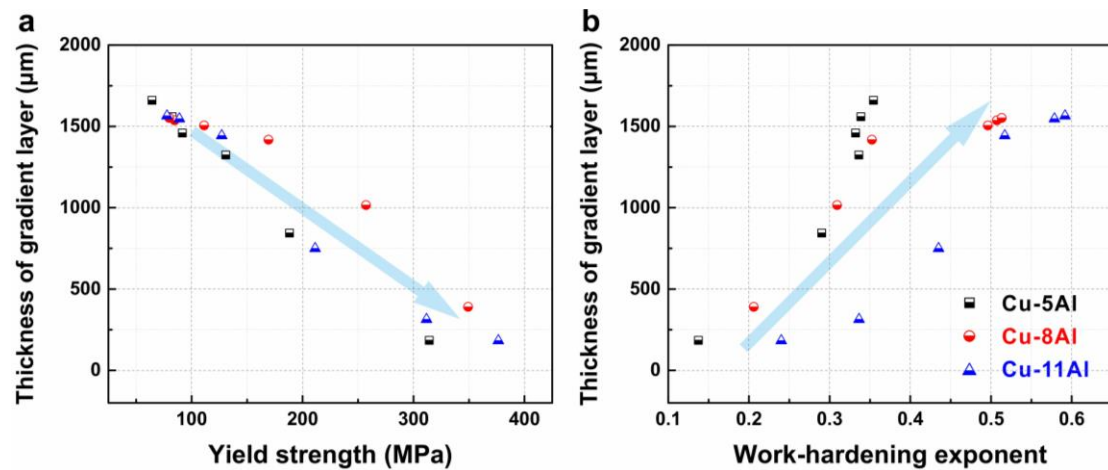


Fig. 9. Thickness of the gradient layer of the 3Sed Cu-Al alloys with different Al contents and matrix grain sizes. (a) Relation between the thickness of the gradient layer and yield strength; (b) relation between the thickness of the gradient layer and work-hardening exponent; (c) relation between the thickness of the gradient layer and grain size.

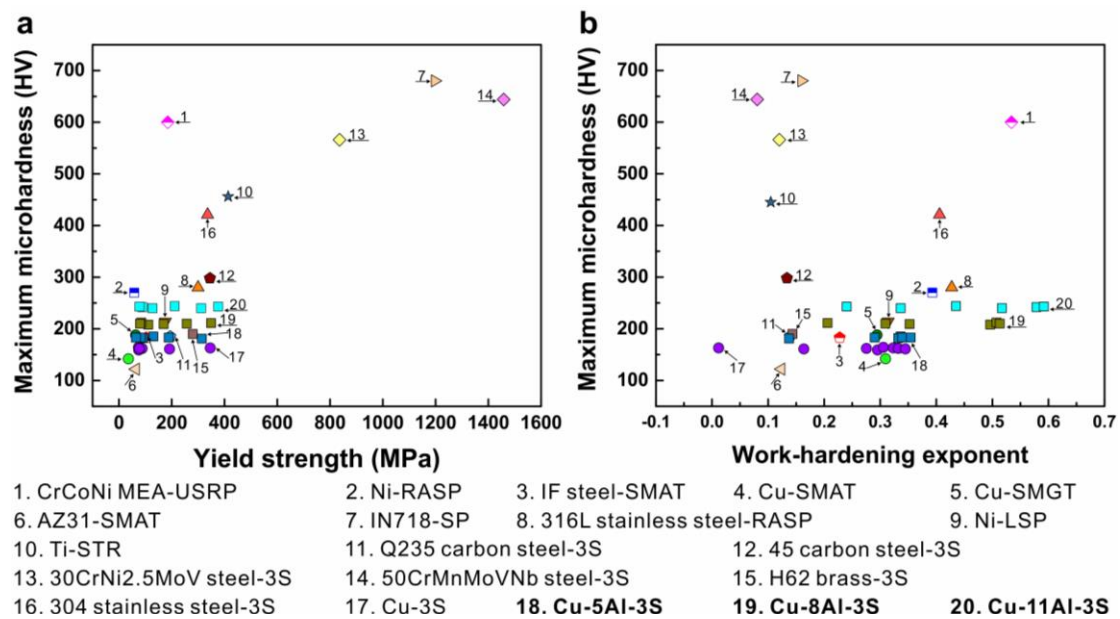


Fig. 10. Maximum microhardness of surface strengthened metallic materials with different chemical components and surface strengthening technologies. (a) Relation between the maximum microhardness and yield strength; (b) relation between the maximum microhardness and work-hardening exponent.

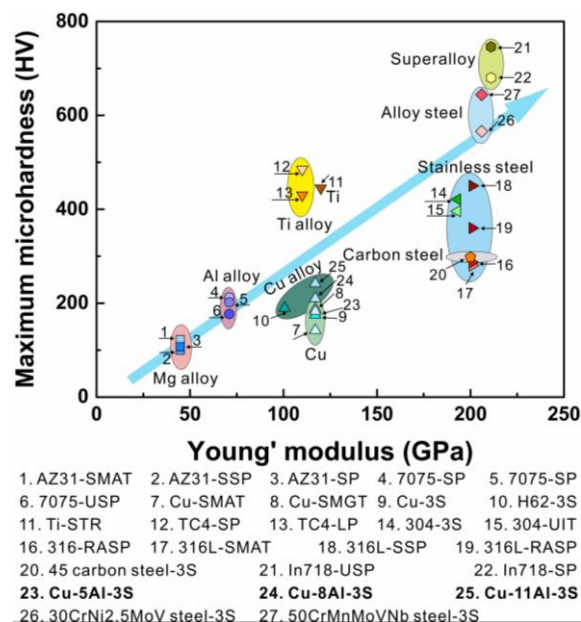


Fig. 11. Relation between the maximum microhardness of the surface strengthened metallic materials and Young's modulus of the corresponding as-received metallic materials.

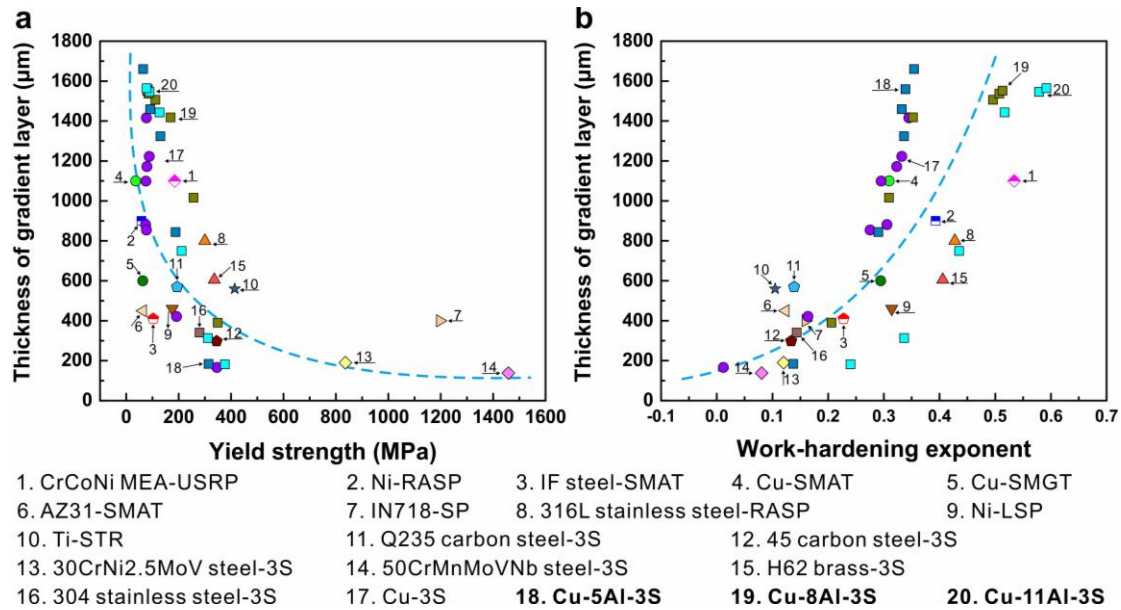


Fig. 12. Thickness of the gradient layer of the surface strengthened metallic materials with different chemical components and surface strengthening technologies. (a) relation between the thickness of the gradient layer of the surface strengthened metallic materials and the yield strength of the corresponding as-received metallic materials; (b) relation between the thickness of the gradient layer of the surface strengthened metallic materials and the work-hardening exponent of the corresponding as-received metallic materials.

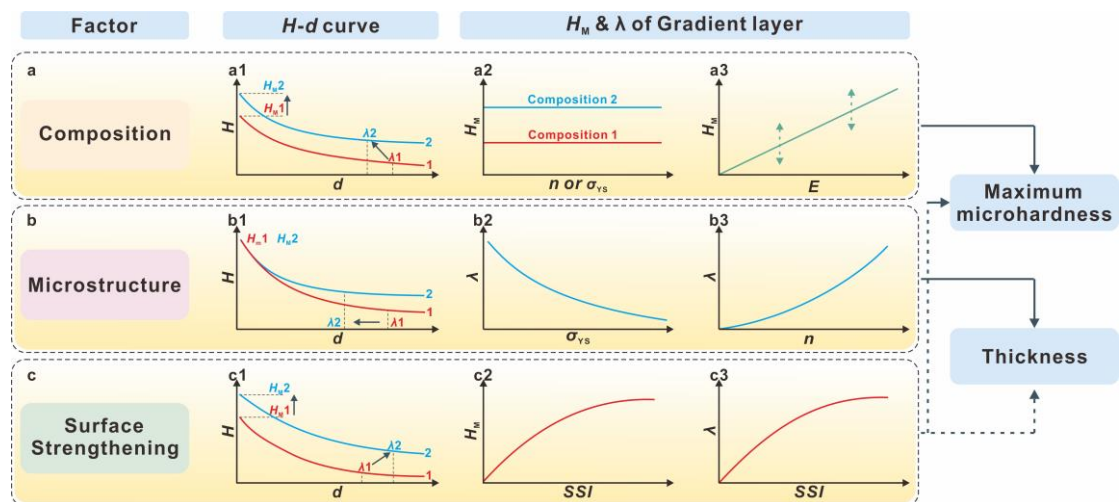


Fig. 13. Schematic illustrations of the effect of composition, microstructure, and surface strengthening on H - d curve and the properties of the gradient layer for the surface strengthened metallic materials, respectively. SSI: surface strengthening intensity.

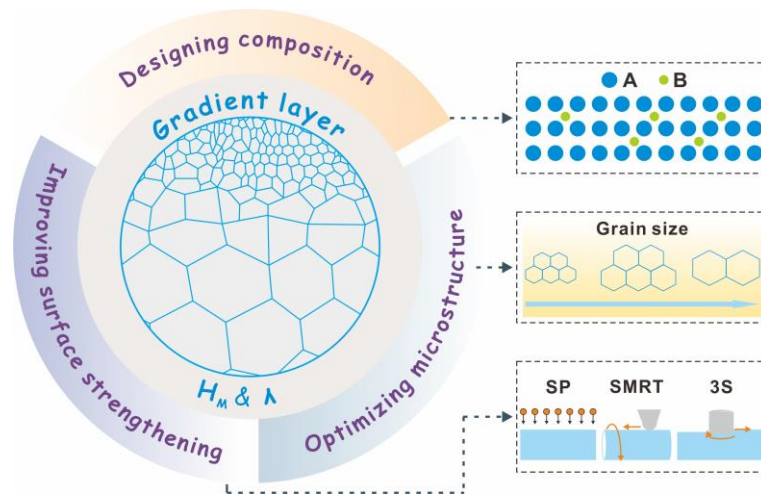


Fig. 14. Schematic illustrations of proposals for improving the properties of the gradient layer of the surface strengthened metallic materials. SP: shot peening; SMRT: surface mechanical rolling treatment; 3S: surface spinning strengthening.